Soft Matter

RSC Publishing

PAPER

View Article Online
View Journal | View Issue

Cite this: *Soft Matter*, 2013, **9**, 7981

A dual-scale model for the caveolin-mediated vesiculation†

Xudong Liang, Yan Zu, Yan-Ping Cao and Chun Yang*

Received 7th April 2013
Accepted 28th June 2013

DOI: 10.1039/c3sm50956g

www.rsc.org/softmatter

Caveolae-mediated vesiculation refers to the ~100 nm cave-like plasma membrane invaginations, which function as macromolecular transport vesicles that regulate cellular function. The initiation of vesiculation is closely associated with protein–protein and protein–membrane interactions, yet their roles in the caveolae budding process are not well-understood. We here propose a dual-scale model, which allows us to identify a unique role for the caveolin–dioleoylphosphatidylserine (DOPS) interaction and the high-order oligomer of caveolins. An energy analysis reveals that the protein–lipid affinity and oligomerization can provide enough energy to increase the local curvature within membrane vesicle formation. Membrane evolution simulations also propose that the radius of the mature vesicle is intrinsic and relies on the molecular interactions, regardless of the oligomer number and surface tension. By introducing molecular interactions at the nanoscale into cellular events occurring in the microscale, the present dual-scale model sheds light on how molecular interactions can change the membrane vesiculation.

1 Introduction

Caveolae are small uncoated pits in plasma membranes that are highly concentrated on primary adipocytes, fibroblasts, muscle cells, and pulmonary type 1 cells as well as endothelial cells.[1] Scanning electronic microscopy (SEM) and the freeze-etch replica technique have revealed a complex filament structure on the surface of caveolae.[2–4] It is believed that the oligomerization of caveolin is composed of filaments and that caveolins serve as the major construction components of caveolae.[5,6] The high-order structure of caveolins induces a bud-like vesicle on membranes with a typical size of ~100 nm.[7] The formation of these vesicles leads directly to macromolecule vesiculation and transportation, thus regulating cellular functions, such as endocytosis, transcytosis, potocytosis[8] and signal transduction.[9]

Recent analysis shows that caveolin mutants, lacking the inter-molecular reaction regions of caveolin-1, are still competent to drive vesicle formation, but result in much larger ones with diameters of up to 1 μm.[10] A puzzle therefore arises of how a nanoscale change in the protein structure could bring about a domino effect on the morphology of vesicles at the microscale.

In order to solve the conundrum of caveolin-mediated vesiculation, efforts have been devoted to establishing biomechanical models, which mainly fall into two brand classes: continuum models and particulate models. The continuum model typically treats the membrane as a two-dimensional linear-elastic sheet in the mesoscale,[11] with membrane-bound caveolins described as polymers grafted to the surface.[12] Lipowsky[13] has extended the continuum model to a multi-polymer system with overlap coverage, which resembles caveolin aggregation in caveolae. Sens and Turner[7] have developed a "blob model" of asymmetrical anchored caveolins to provide the force distribution in caveolae, which explains the formation of a bud-like structure on the membrane. The particulate model accounts for the detailed description of individual atoms of the lipid bilayer and caveolin. The inter-molecular reactions in the particulate model are investigated in the nanoscale with molecular dynamics (MD) or Monte Carlo (MC) methods.[14]

The continuum model has managed to provide a global understanding of caveolae invagination. However, it ignores the details of the inter-molecular reaction. The fully atomic particulate model describes the nanoscale behaviours, but fails to sustain the timescale of vesicle formation up to a microsecond under current computational power.[14] Together, these aforementioned models do not bridge the gap between nanoscale molecular events and microscale membrane behaviours.

A better understanding of the effect of nanoscale events on the microscale morphology requires knowledge of the molecular structure and the interactions. The caveolin protein is a 22 kDa integral membrane protein, which is believed to form a hairpin structure inserted in the lipid bilayer.[15] The two termini, strongly attached to the cell membrane, are composed of a 101 amino-acid polypeptide of the N-terminus tail, and a shorter 44 amino-acid of the C-terminus.[16] Residues 61–101 in the N-terminus are the region corresponding to the formation of

Institute of Biomechanics and Medical Engineering, Department of Engineering Mechanics, Tsinghua University, Beijing, 100084, China. E-mail: yangchun@tsinghua.edu.cn; Tel: +86 10 62788113

† Electronic supplementary information (ESI) available. See DOI: 10.1039/c3sm50956g

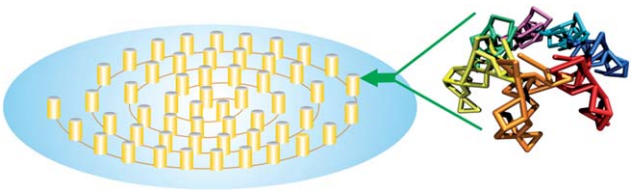

Fig. 1 A schematic of the caveolae structure on the membrane and the structure of caveolin oligomer.[18] Caveolae is a high-order structure composed of caveolin oligomers (yellow cylinders) aligned on the membrane. The caveolin oligomers contain seven caveolins connected by inter-molecular reaction at the N-terminus.[18]

caveolin oligomers, which could assemble into filaments[17] on the caveolae surface (Fig. 1). Additionally, residues 82–101 also bind to the acidic membrane lipids such as dioleoylphosphatidylserine (DOPS) and phosphatidylinositol-4,5-bisphosphate (PIP2)[18] through the non-specific electrostatic interaction,[19] and form membrane domains enriched with DOPS and PIP2.[18]

In the present work, we propose a dual-scale model to overcome the difficulties encountered within the single scale models, and to investigate the process of caveolin-mediated vesiculation. A nanoscale model is built to describe the local curvature promoted from the protein–lipid and protein–protein interactions, and it is coupled with a field-theoretic microscale model[20,21] that predicts the evolution of the membrane as a continuum sheet. The two models of different scales are fused together *via* the local curvature, which is inherited from the nanoscale lipid bilayer and influences the microscale membrane morphology.

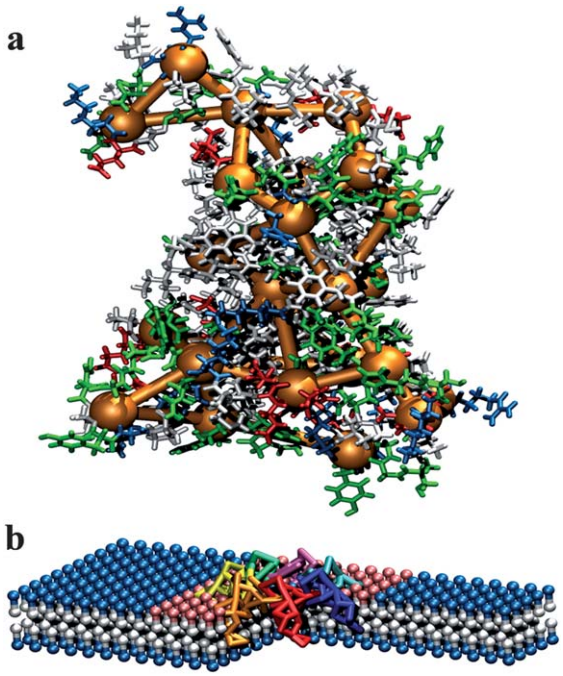

Fig. 2 Shape-based coarse graining (SBCG) methods in the caveolin–lipid structure. (a) Overlap of the all-atom and SBCG models for the caveolin structure. The all-atom structure is drawn using the liquorice representation; while the SBCG model is represented by brown ball-stick model, composed of 25 beads, each containing ~120 atoms. (b) The configuration of caveolin–lipid assembling in coarse grained models. The tail beads of coarse-grained lipid are white, and the head beads of DOPS and DOPC are in pink and blue, respectively. The caveolin oligomer is drawn using 7 different colours.

2 Model and simulation method

2.1 Coarse-grained model for local curvature

The timescale of vesicle formation normally extends to several microseconds,[22] which is not accessible for atomic simulation, of which the time step is about 1–2 fs. Thus, we treat a group of atoms as pseudo-beads[23] to create a coarse-grained caveolae membrane system, which retains a much larger timescale of 100 fs.[24] As the atomic coordinate of caveolin is as yet unavailable in the Protein Data Base,[25] we refer to the predicted protein structure based on sequence homology modelling.[26,27] Residues 1–151 in caveolin are computed according to the template structure of elongation factor 3 (PDB ID 2IW3)[28] in the Protein Model Portal.[29] The coarse graining process is carried out using the program VMD[30] with shape-based coarse graining (SBCG) methods.[31] The caveolin structure topology is reserved, and the molecule is divided into 25 beads, each containing about 120 atoms (Fig. 2a). The mass and the charge of each bead are inherited from the correspondent atoms in each group. A bond between two beads is established provided that their distance is within 2.5 nm. A CHARMM-style force field[31] is used to calculate the interaction potential of the coarse-grained beads. The non-bonded potentials are constituted from the 6-12 Lennard-Jones (LJ) potential and the Coulomb terms, whereas the bonded potentials are represented by the harmonic bonds and the angle potentials (without the dihedral potentials).[31]

The coarse-grained (CG) membrane consists of dioleoylphosphatidylcholine (DOPC) and DOPS.[31] Each lipid consists two connected beads, one head and one tail bead. The coarse-grained lipid contains 2.2 lipid molecules, giving 150 atoms per bead, and the size of which is similar to that of caveolin. The DOPC lipid is neutral in charge, whereas the DOPS lipid has a negative charge of −2.2 e on each head bead. Full technological details of the membrane model can be found in ref. 31 and the self-assembly dynamics of the lipid membrane in Fig. S1.† The estimated amount of DOPS in each lipid patch is about 20% of all the lipid components, referring to the work of Wanaski *et al.*,[18] and it is distributed around the caveolin oligomer as a DOPS enriched domain[18] which interacts with the caveolin scaffolding region *via* non-specific electrostatic interactions.[19] According to the caveolae filament subunit model,[17] the caveolin–lipid system is assembled as a heptameric ring of caveolin monomers and embedded within the membrane. The trans-membrane domains of caveolins are buried in the membrane[15,16] as shown in Fig. 2b. Ions (such as Na^+ and Cl^-) with hydration shells[31] are added to the system to balance the charge, and their initial positions are randomly chosen in the simulation volume.

We performed all the coarse-grained simulations with the parallel MD program NAMD 2.8.[32] A periodic condition was adopted in all of the simulations with a single time step of 100 fs and a 3 nm cut-off for non-bonded interactions. An energy

minimization was taken for 10^4 steps; and then the simulation was run for 5×10^6 steps, corresponding to the timescale of 0.5 μs, at the temperature of 310 K.

2.2 Field-theoretic approach in caveolae vesiculation

Field-theoretic approach focuses on the energetic and entropic contribution to continuum membrane models,[21,33] linking the membrane shape with the elastic energy, E, *via* the Canham–Helfrich Hamiltonian:[11]

$$E = \sigma \Delta A + \int \frac{\kappa}{2} J^2 \mathrm{d}A \quad (1)$$

where $\sigma\Delta A$ is the energy associated with the membrane stretching, depending on the membrane tension σ, and the change in its surface area ΔA. The second term is the integral of the membrane bending energy over the whole surface area A. J is a function of membrane curvature, and κ represents the membrane bending rigidity.

Under the axis-symmetry assumption of vesicles, the cell membrane is simplified into a one-dimensional structure, the deformation of which is governed by the following equations:[33]

$$\begin{aligned} \psi''(s) &= \frac{\cos\psi \sin\psi}{R^2} - \frac{\psi' \cos\psi}{R} + \frac{\nu \sin\psi}{R\kappa} + H_0'(s) \\ \nu'(s) &= \frac{\kappa(\psi' - H_0)^2}{2} - \frac{\kappa \sin^2\psi}{2R^2} + \sigma \\ R'(s) &= \cos\psi \\ Z'(s) &= -\sin\psi \end{aligned} \quad (2)$$

where s is the arc-length along the contour and $\psi(s)$ the membrane angle (Fig. S2†). $R(s)$ and $Z(s)$ represent the Cartesian coordinates in the x–z plane. $\nu(s)$ is the Lagrange multiplier introduced to satisfy the constraint $R'(s) = \cos\psi$. $H_0(s)$ is the initial local curvature of the membrane induced by the molecular interaction. Considering the pinning of membrane by the cytoskeleton[33] at the boundary, $\psi = 0$ at $R = R_0$ (or at $s = s_1$). Due to the axis-symmetry property, the membrane angle $\psi = 0$ at $R = 0$. An additional equation is specified as $\nu(s_1) = \sigma R_0$.[33] Here, we take $R_0 = 500$ nm and the membrane surface tension ranging from 0–10^{-5} N m^{-1} (0–0.001 pN nm^{-1}). A shooting method was used to find the desired solution to meet the boundary conditions.

3 Results

3.1 Local curvature from the coarse-grained simulation

To study the local membrane curvature induced by the caveolin oligomerization and the caveolin–DOPS interaction, three cases of coarse-grained simulations are investigated: (1) the heptameric ring of caveolins located at the centre of a membrane with concentrated DOPS around the proteins on the cytosolic side (Fig. 3a, SET1 for later reference); (2) the de-oligomerized caveolin monomers distributed randomly on the cytosolic side of the membrane with concentrated DOPS around the proteins (Fig. 3c, SET2 for later reference); and (3) the heptamer embedded at the centre of a membrane with scattered DOPS (Fig. 3e, SET3 for later reference). The local curvatures of the simulated lipid bilayer are calculated from the membrane shape projected on the cross-section parallel to the x–z plane, similar to Blood and Voth.[34] In detail, the head groups of the lipids in the inner leaflet underneath the caveolin oligomer are projected to the cross-section (Fig. 4a), and the average curvature is derived from the quadratic fitting curve of the head groups every 0.05 μs.

In SET 1, the protein–lipid configuration is adopted from experimental observations of the oligomerized caveolin structure[17] and the clustering of DOPS in the presence of the caveolin scaffolding domain.[18] This configuration is expected to capture the basic molecular structure of the real membrane. During the course of the simulation, the caveolin oligomer structure is held intact. All the independent simulations have revealed an imperceptible curving after a period of energy minimization. And then an undulation of the lipids happens around the caveolin oligomer-occupied region and develops into a visible membrane bending (Fig. 3b) at the end of the simulation. Fig. 4b reveals an increasing trend of membrane curvature, which is stabilized into a range from 0.05 to 0.09 nm^{-1} after 0.3 μs. The fluctuation of the local curvature can be attributed to the random distribution of ion hydration shells.

Taking a different configuration of the caveolins and lipids, SET2 and SET3 lead to a much lower scale of membrane bending in the simulations, as the oligomerization of caveolin and clustering of DOPS is disrupted, respectively. SET3 reveals the lowest curvature during the course of the simulation (Fig. 4b). The pattern of the lipid distribution in SET3 disrupts the caveolin–DOPS interaction by inserting DOPC around the caveolin oligomers, making the membrane flattened through the simulation with an average curvature lower than 0.01 nm^{-1} (Fig. 3f). This prediction suggests that oligomerization of caveolin alone cannot induce the membrane curving in the absence of the caveolin–DOPS interaction. Compared to SET1 and SET3, SET2 shows a moderate curving in the membrane as the caveolin oligomer is replaced by a random distribution of the caveolin monomers during the simulation (Fig. 3d and 4b). The rebuilding of the caveolin–DOPS interaction seems to provide sufficient energy for the membrane bending to the degree of 0.04 nm^{-1} at a steady stage (after 0.3 μs). However, the de-oligomerization of caveolin impedes a further deformation of the membrane.

The caveolin oligomerization and the caveolin–DOPS interaction have been observed in caveolin-dependent endocytosis.[17,18] However, the roles of the protein–protein or protein–lipid interactions in the dynamics of the endocytosis are not well illustrated. To understand the mechanism of the molecular interaction affecting the membrane bending, we analyse the system's energy through the period of simulation. The initial value of each line (Fig. 5) is calculated after energy minimization in the MD simulation, and represents the system energy brought by the topology of the caveolin oligomers and DOPS distribution. The system energy gradually descends to a steady value at the end of the simulation, as the average curvature development. The caveolin oligomers and DOPS distribution in SET1 provide the highest energy input compared to SET2 and SET3, indicating that the topological distribution of molecules stimulates the formation of membrane curving. The steady

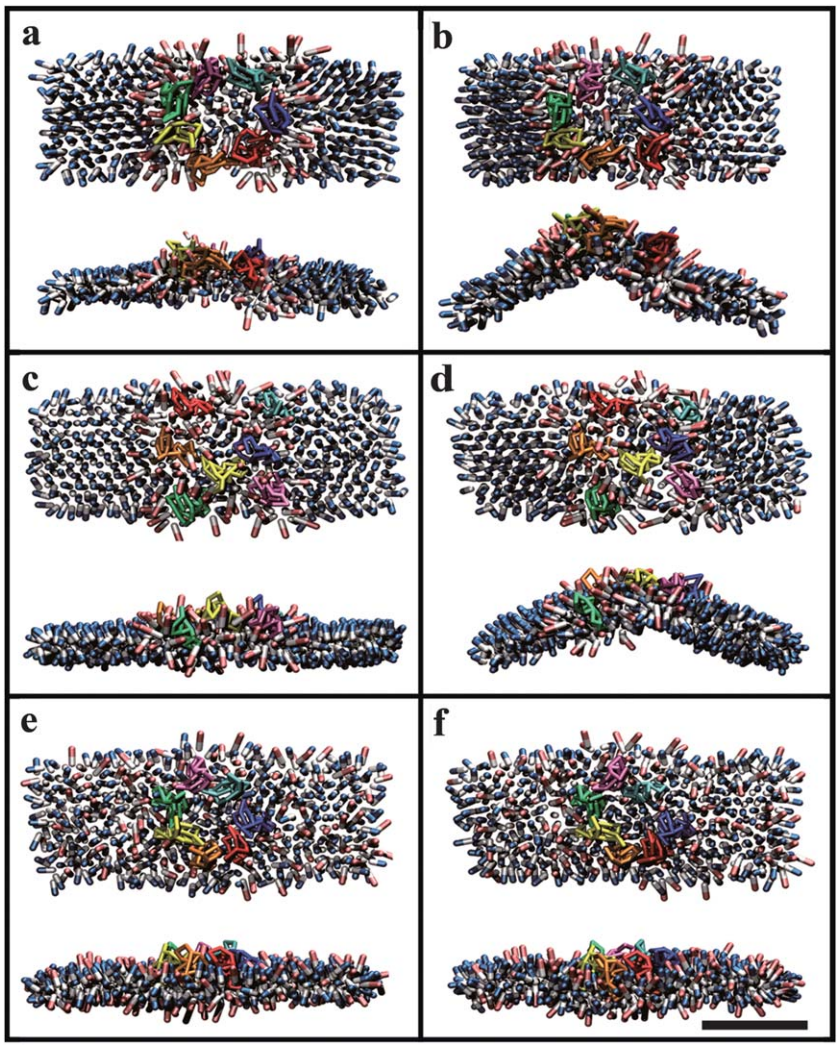

Fig. 3 The top and horizontal views of caveolin–lipid models in coarse-grained simulation: (a) and (b) represent the initial and the final configurations of SET1, respectively; (c) and (d) for SET2; and (e) and (f) for SET3. The scale bar represents 10 nm.

energy of the systems reveals the contribution of the molecular interaction, *i.e.*, the intermolecular reactions direct the membrane morphology to an energetically favourable position during the simulation. The strong molecular interaction resulting from the DOPS concentration in SET 1 and SET2 induces a remarkable curvature increment over SET3. In summary, our present molecular simulations and energy analysis suggest that membrane bending behaviour is closely associated with two factors: (1) the molecular topology of the caveolin oligomers and the DOPS concentration, and (2) the caveolin–DOPS interaction.

3.2 Microscale vesiculation of caveolae

To understand the effect of nano events upon caveolae vesiculation, we introduce the local curvature provided by the coarse-grained simulations into the continuum membrane governing eqn (2) as the membrane's initial local curvature $H_0(s)$. Previous studies[35,36] have demonstrated that the membrane morphology is not sensitive to the form of $H_0(s)$, but sensitive to the magnitude of the local curvature. Further coarse-grained simulations also reveal that the average magnitude of the local curvature is not affected by the presence of neighboring oligomers (Fig. S3 and S4† for the case of three oligomers). We thus adopt $H_0(s) = C_0 e^{-s^2/b^2}$ to fit the shape of the membrane patch extracted from the single oligomer CG simulation (Fig. S5†). For SET1, we have obtained $C_0 = 0.08\ \text{nm}^{-1}$ and $b = 7.7$ nm; and $C_0 = 0.04\ \text{nm}^{-1}$ and $b = 7.5$ nm in SET2. The curvature of SET3 is imperceptible since it is too small to induce a membrane vesiculation.

The curvature field is composed of local curvatures aligned in a spiral filamentous manner on the membrane.[5,6,17] According to the negative-stain electronic microscopy results, the average distance between the adjacent oligomers is taken as 20 nm.[17] Therefore, within the axis-symmetric membrane model,[33] H_0 is

$$H_0(s) = \sum_i C_0 e^{-\left(s - s_{0,i}\right)^2/b^2} \quad (3)$$

where s_0 is the centre of each oligomer, and the index i represents the sequence of oligomer aligned in the radial direction

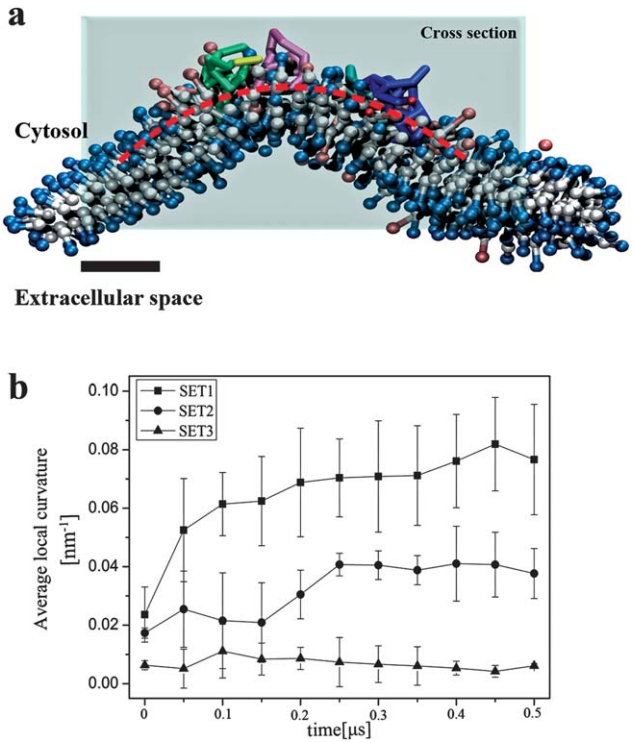

Fig. 4 (a) The lipid bilayer dissected by a cross-section parallel to the *x*–*z* plane. The local curvature was extracted from lipid head groups of the inner leaflet, which is fitted with quadratic functions (red dashed line). The scale bar represents 5 nm. (b) Average curvatures derived from the quadratic fitting curve of the head groups in SET1, SET2 and SET3, respectively.

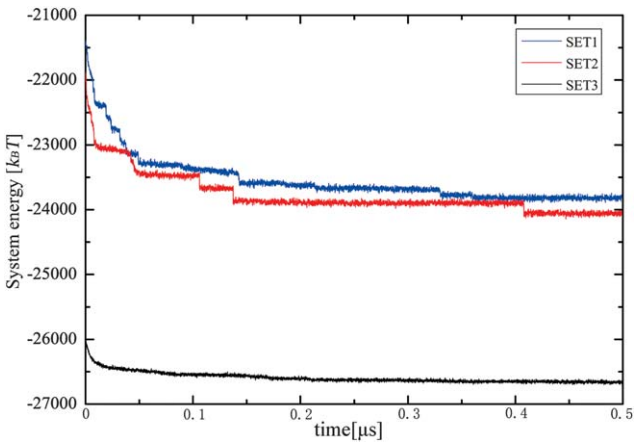

Fig. 5 Energy distributions of caveolin–lipid models. The configuration of caveolin oligomer and DOPS concentration induced the highest energy input and the stabilized energy in SET1. SET2 showed lower ones as the oligomer was disrupted, and the energy in SET3 was the lowest due to the random distribution of DOPS.

every 20 nm. In Fig. 6, we depict the membrane shapes in cells under the influence of the local curvature imposed by the caveolin oligomers. As the number of oligomers increases, the morphology of the budding membrane changes from a small bulge into a bottle-like mature vesicle. At least 9 consecutive oligomers are required to establish a vesicle with a narrowed neck (Fig. 6), which is believed to be the mature one resembling

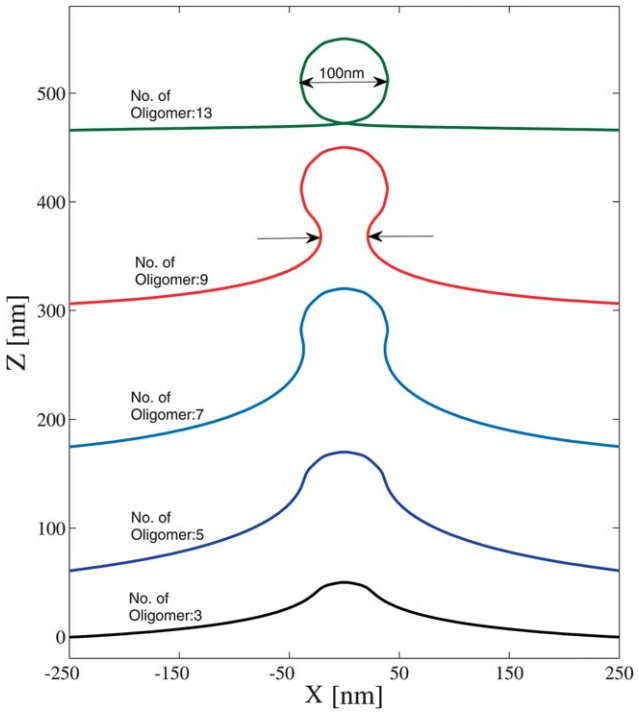

Fig. 6 Membrane shape under the influence of local curvature imposed by caveolin oligomers. The membrane evolves from a small bulge to a vesicle with a narrow neck (black arrows) as the number of aligned oligomers increases.

the experimental observation.[37] The neck gradually disappears as the number of oligomers increases to 13. Therefore, the evolution of the membrane is highly dependent on the number of caveolin oligomers. However, the radius of the growing buds is insensitive to the number of the imposed curvatures as the diameter of the vesicles is steady at 100 nm (Fig. 6).

For biological membranes, the bending rigidity is believed to have a value of 20 k_BT.[38] However, the surface tension of the cell membrane varies in cell types because of the differences in the mechanical environment, *i.e.* the osmotic pressure and the external forces applied on the cells.[39] Hence, we have explored the effect of the surface tension ranging from 0 to 10^{-5} N m^{-1} (0–0.001 pN nm^{-1}) on the membrane shape.[40] The local curvature is taken from SET1 and the number of the caveolin oligomers is 9. The predicted membrane profiles with different surface tensions are plotted in Fig. 7, demonstrating an imperceptible influence of the surface tension on the membrane profiles, *i.e.*, the size and the shape of the budding vesicles remain unchanged.

As for the mutated cells in which caveolins are de-oligomerized, the local curvature induced by the molecular interactions is just one-half of that in normal cells (Fig. 4b). The attenuated local curvature leads to a larger vesicle with a diameter of 200 nm (Fig. 8). Accordingly, the number of the local curvature imposed by the clusters of de-oligomerized caveolins also increases, *i.e.*, 17 clusters are required in forming a mature vesicle with a narrowed neck. This agrees with the previous reports that the mutation in the self-attractive segment of caveolin N-termini (responsible for the formation of oligomers) results in much larger buds with diameters up to 1 μm.[10]

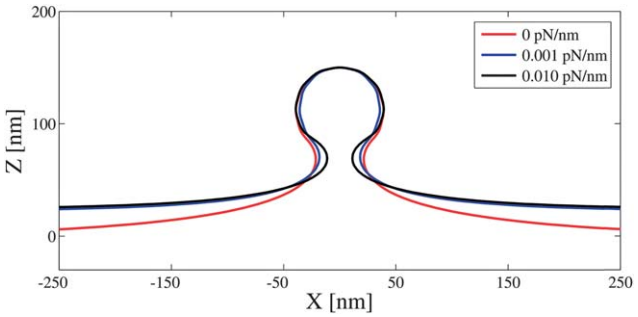

Fig. 7 Shapes of membranes with the surface tension ranging from 0 to 10^{-5} N m^{-1}. The local curvature was imposed by 9 aligned caveolin oligomers. The surface tension was taken as 0, 10^{-6} and 10^{-5} N m^{-1}, which induced an undetectable variation of the mature vesicle profiles.

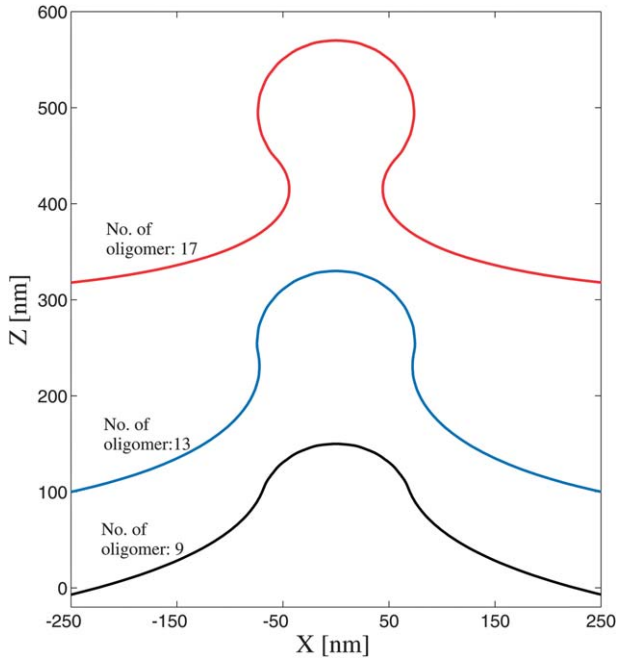

Fig. 8 Membrane shape under the influence of local curvature imposed by de-oligomerized caveolins in the mutated cells. The weak local curvature led to the formation of larger mature vesicles with a diameter of 200 nm.

These results provide a perspective that the radius of the mature vesicles is independent of the number of the local curvatures imposed by the caveolin oligomers and the surface tension, but relies strongly upon the caveolin oligomerization. The critical diameters of the vesicles induced by the oligomerized or de-oligomerized caveolin are 100 nm and 200 nm, respectively. This is in good agreement with previous experimental results,[10,17] and indicates that the strength of molecular interactions determines the radius of the vesicles.

4 Concluding remarks

In conclusion, we have presented a dual-scale model of caveolin-mediated vesiculation, which involves a nanoscale description of the local curvature imposed by the molecular interactions, and a microscale model of the membrane evolution under the energy minimization process. Starting from the coarse-grained membrane model, we predict that the curvature-mediated behaviours of the membrane are influenced by molecular interactions. Instead of simulating the membrane remodelling with a full coarse-grained model,[41] we introduced the field-theoretic method to capture the key morphological changes in the microscale membrane vesiculation. With the present dual-scale model, we can provide a panoramic understanding of vesicle formation without losing the details of the molecular structure and interactions. By bridging the two scales with the local curvature, our model provides a method to explore how a nanoscale change in the protein structure could bring about a domino effect on the morphology of vesicles at the microscale with reasonable accuracy.

We have identified a critical radius of caveolin-dependent vesicles. According to the model, the vesicle evolution shows a strong dependence upon the number of caveolin oligomers. However, the radius of the vesicles is independent of the oligomer number and the surface tension, and relies upon the molecular interactions that are predetermined by the protein and lipid configuration. Thus the critical radius is believed to be an intrinsic property of the membrane and may explain the prevalence of caveolae-dependent endocytosis in different cell types. For caveolin-mediated vesicles in normal or mutated cells, the intrinsic diameter is 100 nm and 200 nm, respectively. The de-oligomerization of caveolin can induce an increase of the intrinsic vesicle diameters in mutated cells.

Based on the membrane bending given by the coarse-grained molecular simulations, we also specify a unique role of the caveolin–DOPS interaction and caveolin oligomerization in the local curvature formation. More specifically, the caveolin–DOPS interaction is found to be fundamental for the bending of the membrane, as a major energy contribution. The disruption of this interaction results in an undetectable local curvature and the subsequent flattened membrane in cells. Therefore, the caveolin–DOPS interaction is essential for vesicle initiation. According to the observation in liposomes,[18] the DOPS enrichment is believed to be due to the caveolin–DOPS interaction. However, such a lipid aggregation process is unable to be seen in the randomly distributed DOPS in SET 3, because the lipid aggregation requires a timescale seemingly much longer than the present nano-scale simulation.

The caveolin oligomerization is believed to enhance the membrane deformation compared to the cluster of the monomers, and the existence of the oligomers may account for this nanoscale difference. The microscale membrane evolution also revealed an important role of the caveolin oligomerization in vesicle formation, namely that the size of the vesicle is profoundly influenced by the local curvature. Compared with normal caveolins, mutated ones cause a weaker interaction in the oligomers, and in turn result in a larger vesicle. This sheds light on the understanding of how a nanoscale mutation in the protein structure could bring about a significant morphological change of the vesicles in the microscale.

Taken together, the present method manages to bridge the gap between the two models of nano- and micro-scales, and emphasizes the effect of molecular interactions on the

membrane morphology. The framework of the dual-scale model can not only help to explain the mechanism of caveolin-mediated vesiculation, but also be adopted as an approach in various situations of the curvature-mediated membrane interactions, ranging from the active cellular behaviour of clathrin-dependent endocytosis, phagocytosis and macropinocytosis, and the invasion of virus[38] and passive transportation of carbon nanotubes (CNTs)[42] into the cells.

Acknowledgements

We thank Profs Xi-Qiao Feng and Shou-Wen Yu for their valuable suggestions on the simulation and analysis. We also thank Dr Neeraj Agrawal for his help in the membrane simulation. This work was supported by the National Natural Science Foundation of China (31170885 and 31000418); Tsinghua University (2011Z02175), and Tsinghua National Laboratory for Information Science and Technology.

References

1 A. Gilbert, J. P. Paccaud, M. Foti, G. Porcheron, J. Balz and J. L. Carpentier, *J. Cell Sci.*, 1999, **112**, 1101–1110.
2 K. R. Peters, W. W. Carley and G. E. Palade, *J. Cell Biol.*, 1985, **101**, 2233–2238.
3 K. G. Rothberg, J. E. Heuser, W. C. Donzell, Y. S. Ying, J. R. Glenney and R. G. W. Anderson, *Cell*, 1992, **68**, 673–682.
4 R. V. Stan, *Microsc. Res. Tech.*, 2002, **57**, 350–364.
5 S. Monier, R. G. Parton, F. Vogel, J. Behlke, A. Henske and T. V. Kurzchalia, *Mol. Biol. Cell*, 1995, **6**, 911–927.
6 M. Sargiacomo, P. E. Scherer, Z. L. Tang, E. Kubler, K. S. Song, M. C. Sanders and M. P. Lisanti, *Proc. Natl. Acad. Sci. U. S. A.*, 1995, **92**, 9407–9411.
7 P. Sens and M. S. Turner, *Biophys. J.*, 2004, **86**, 2049–2057.
8 J. E. Schnitzer, P. Oh, E. Pinney and J. Allard, *J. Cell Biol.*, 1994, **127**, 1217–1232.
9 M. P. Lisanti, P. E. Scherer, Z. Tang and M. Sargiacomo, *Trends Cell Biol.*, 1994, **4**, 231–235.
10 S. W. Li, F. Galbiati, D. Volonte, M. Sargiacomo, J. A. Engelman, K. Das, P. E. Scherer and M. P. Lisanti, *FEBS Lett.*, 1998, **434**, 127–134.
11 W. Helfrich, *Z. Naturforsch., C: J. Biosci.*, 1973, **28**, 693–703.
12 P. G. De Gennes, *Scaling Concepts in Polymer Physics*, Cornell University Press, Ithaca, NY, 1st edn, 1979.
13 R. Lipowsky, *Colloids Surf., A*, 1997, **128**, 255–264.
14 G. Brannigan, L. C. L. Lin and F. L. H. Brown, *Eur. Biophys. J. Biophys. Lett.*, 2006, **35**, 104–124.
15 P. Dupree, R. Parton, T. V. Kurzchalia and K. Simons, *Mol. Biol. Cell*, 1992, **3**, A308.
16 A. Schlegel, R. B. Schwab, P. E. Scherer and M. P. Lisanti, *J. Biol. Chem.*, 1999, **274**, 22660–22667.
17 I. Fernandez, Y. S. Ying, J. Albanesi and R. G. W. Anderson, *Proc. Natl. Acad. Sci. U. S. A.*, 2002, **99**, 11193–11198.
18 S. P. Wanaski, B. K. Ng and M. Glaser, *Biochemistry*, 2003, **42**, 42–56.
19 N. BenTal, B. Honig, R. M. Peitzsch, G. Denisov and S. McLaughlin, *Biophys. J.*, 1996, **71**, 561–575.
20 E. M. Lennon, K. Katsov and G. H. Fredrickson, *Phys. Rev. Lett.*, 2008, **101**, 138302.
21 U. Seifert, *Adv. Phys.*, 1997, **46**, 13–137.
22 P. J. Bond, J. Holyoake, A. Ivetac, S. Khalid and M. S. P. Sansom, *J. Struct. Biol.*, 2007, **157**, 593–605.
23 S. O. Nielsen, C. F. Lopez, G. Srinivas and M. L. Klein, *J. Phys.: Condens. Matter*, 2004, **16**, R481–R512.
24 A. Arkhipov, P. L. Freddolino and K. Schulten, *Structure*, 2006, **14**, 1767–1777.
25 H. M. Berman, J. Westbrook, Z. Feng, G. Gilliland, T. N. Bhat, H. Weissig, I. N. Shindyalov and P. E. Bourne, *Nucleic Acids Res.*, 2000, **28**, 235–242.
26 J. M. Chandonia and S. E. Brenner, *Science*, 2006, **311**, 347–351.
27 J. Liu, G. T. Montelione and B. Rost, *Nat. Biotechnol.*, 2007, **25**, 849–851.
28 C. B. F. Andersen, T. Becker, M. Blau, M. Anand, M. Halic, B. Balar, T. Mielke, T. Boesen, J. S. Pedersen, C. M. T. Spahn, T. G. Kinzy, G. R. Andersen and R. Beckmann, *Nature*, 2006, **443**, 663–668.
29 K. Arnold, F. Kiefer, J. Kopp, J. N. D. Battey, M. Podvinec, J. D. Westbrook, H. M. Berman, L. Bordoli and T. Schwede, *J. Struct. Funct. Genomics*, 2009, **10**, 1–8.
30 W. Humphrey, A. Dalke and K. Schulten, *J. Mol. Graphics Modell.*, 1996, **14**, 33–38.
31 A. Arkhipov, Y. Yin and K. Schulten, *Biophys. J.*, 2008, **95**, 2806–2821.
32 J. C. Phillips, R. Braun, W. Wang, J. Gumbart, E. Tajkhorshid, E. Villa, C. Chipot, R. D. Skeel, L. Kale and K. Schulten, *J. Comput. Chem.*, 2005, **26**, 1781–1802.
33 N. J. Agrawal, J. Nukpezah and R. Radhakrishnan, *PLoS Comput. Biol.*, 2010, **6**, e1000926.
34 P. D. Blood and G. A. Voth, *Proc. Natl. Acad. Sci. U. S. A.*, 2006, **103**, 15068–15072.
35 N. J. Agrawal, J. Weinstein and R. Radhakrishnan, *Mol. Phys.*, 2008, **106**, 1913–1923.
36 J. Liu, R. Tourdot, V. Ramanan, N. J. Agrawal and R. Radhakrishanan, *Mol. Phys.*, 2012, **110**, 1127–1137.
37 R. Parton, M. Bayer and J. Hancock, *J. Cell Sci.*, 2005, **119**, 787–796.
38 H. Gao, W. Shi and L. B. Freund, *Proc. Natl. Acad. Sci. U. S. A.*, 2005, **102**, 9469–9474.
39 B. Sinha, D. Köster, R. Ruez, P. Gonnord, M. Bastiani, D. Abankwa, R. V. Stan, G. Browne, B. Vedie, L. Johannes, N. Morone, R. G. Parton, G. Raposo, P. Sens, C. Lamaze and P. Nassoy, *Cell*, 2011, **144**, 402–413.
40 S. Morlot, V. Galli, M. Klein, N. Chiaruttini, J. Manzi, F. Humbert, L. Dinis, M. Lenz, G. Cappello and A. Roux, *Cell*, 2012, **151**, 619–629.
41 B. J. Reynwar, G. Illya, V. A. Harmandaris, M. M. Müller, K. Kremer and M. Deserno, *Nature*, 2007, **447**, 461–464.
42 D. Cui, F. Tian, C. S. Ozkan, M. Wang and H. Gao, *Toxicol. Lett.*, 2005, **155**, 73–85.